International Journal of Thermal Sciences 49 (2010) 1010–1018

Contents lists available at ScienceDirect

International Journal of Thermal Sciences

journal homepage: www.elsevier.com/locate/ijts

Effect of wall proximity on forced convection in a plane channel with a built-in triangular cylinder

Mousa Farhadi*, Kurosh Sedighi, Afshin Mohsenzadeh Korayem

Faculty of Mechanical Engineering, Babol University of Technology, Babol, Islamic Republic of Iran

ARTICLE INFO

Article history:
Received 23 January 2009
Received in revised form
23 December 2009
Accepted 23 December 2009
Available online 4 February 2010

Keywords:
Triangular cylinders
Wall proximity
Convective heat transfer

ABSTRACT

A numerical investigation has been carried out to analyze the effect of wall proximity of a triangular cylinder on the heat transfer and flow field in a horizontal channel. Computations have been carried out for Reynolds numbers (based on triangle width) range of 100–450 and gap widths (a/h) 0.5, 0.75 and 1. Results are presented in the form of instantaneous contours of temperature, vorticity, with some characteristics of fluid flow and heat transfer; such as time-averaged and instantaneous local Nusselt number, skin friction coefficient along bottom channel's wall, and drag coefficient. Results show that approaching triangular cylinder in the wall, removes vortex shedding and subsequently the heat transfer rate decreases at low Reynolds number. By decreasing the vortex shedding, drag coefficient decrease as triangular cylinder approaches the wall of the channel. The variation of vortex formation has a more significant suppression effect on the skin friction coefficient than the Nusselt number.

1. Introduction

The flow passing through a bluff body placed in the channel has been one of the most interested topics and occurs in many engineering applications such as the cooling of electronic components and heat exchangers. Enhancement of heat transfer by a bluff body placed in channel with devices leaves a topic of interest and has been investigated by researchers [1–6]. Wang et al. [3] reported that significance increase in heat transfer occurs as the flow becomes unsteady for a channel that has built in-line and staggered ribs. They reported that for an in-line case, the flow become unsteady at Reynolds number around 110 while for the staggered case this value is around 200. Valencia [4] computed the flow and heat transfer in a channel wall for fully developed channel flows with a built-in tandem of rectangular cylinders placed perpendicular to the flow direction in the channel center plane. Data for heat transfer and flow losses are presented for $100 \leq Re \leq 400$ and the cylinder separation distance $1 \leq S/H \leq 4$. He computed the heat transfer enhancement on the channel walls is about 78% for $S/H = 2$, 3 and 4 at $Re = 400$. Abbassi et al. [5] carried out a numerical investigation to study forced convection of air for a two-dimensional unsteady-laminar flow in a horizontal channel with a built-in triangular prism. They showed that the presence of triangular prism for symmetric flow ($Re < 45$) has just a little local effect on heat transfer from the channel wall. In contrast the periodic flow ($Re \geq 45$) presence with triangular prism has an important effect in enhancement of heat transfer from the channel wall. Heat transfer also increases strongly with Reynolds number so that order of enhancement of average Nusselt number is 85% at $Re = 250$. Chattopadhyay [6] studied the same geometry in the turbulence regime. In this case an augmentation of about 17% in averaged Nusselt number is recorded.

The problem of a bluff body in the vicinity of wall and effect of wall proximity has been studied in the past; most of the research is directed toward the fluid mechanics studies and especially for a square or rectangular and circular cylinder ([1,7–13]). The laser Doppler velocimetry (LDV) study of Ulrichs and Herwig [7] over a right-angled triangle about the separation behavior of bluff bodies in the vicinity of a wall showed that when a triangle is placed in the vicinity of the wall there will be two separation regions: (i) bluff body separation region (ii) wall bounded separation region. As a triangle moves away from the wall, the wall bounded separation region eventually disappears. When bluff body is placed in the center of channel we will have a periodic flow pattern (of alternating vortices). As the bluff body approaches the wall the flow in the cylinder wake becomes increasingly asymmetric and for sufficiently small gap widths, the periodic motion is completely suppressed. This critical gap width depend on the boundary layer thickness (δ/D) and Reynolds number. It has been reported different critical gaps width by authors at high Reynolds numbers. An LDV study by Durao et al. [8] on a square cylinder

* Corresponding author at: Faculty of Mechanical Engineering, Babol University of Technology, Babol, P.O. Box 484, Islamic Republic of Iran. Tel.: +98 111 3234205; fax: +98 111 3234201.
E-mail addresses: mfarhadi@nit.ac.ir (M. Farhadi), ksedighi@nit.ac.ir (K. Sedighi), Af.mohsenzadeh@gmail.com (A. Mohsenzadeh Korayem).

1290-0729/$ – see front matter © 2010 Elsevier Masson SAS. All rights reserved.
doi:10.1016/j.ijthermalsci.2009.12.013

Nomenclature

a	Distance of the apex of triangle from the bottom wall of channel (m)
B	Triangle width (m)
a/h	Gap width ratio
C_f	Skin friction coefficient, $2(\partial u/\partial y)_W/\mathrm{Re}$
C	Modified skin friction coefficient; $C_f \cdot \mathrm{Re}$
$\langle\overline{C}\rangle$	Streamwise and time-averaged Modified skin friction coefficient
C_d	Drag Coefficient,
f	Eddy-shedding frequency
H	Channel width (m)
h	Half of the channel width (H/2), m
Nu	Local Nusselt number, $\partial\theta/\partial y\|_{y=0}$
$\overline{\mathrm{Nu}}$	Streamwise averaged Nusselt number
$\langle\overline{\mathrm{Nu}}\rangle$	Streamwise and time-averaged Nusselt number
p^*	Pressure, pa
p	Dimensionless pressure, $p^*/\rho u_{\max}^2$
Pr	Prandtl number
Re	Reynolds number, $u_{\max}\cdot B/\nu$
Sr	Strouhal number, $f\cdot B/u_{\max}$
T	Temperature (K)
t	Time(s)
U	Mean dimensionless velocity
(u^*,v^*)	Velocity components
u, v	Dimensionless velocity, $(u^*,v^*)/u_{\max}$
(x^*, y^*)	Cartesian coordinates
(x, y)	Dimensionless coordinates, $(x^*,y^*)/B$

Greek symbols

τ	Dimensionless time, $t\cdot u_{\max}/B$
θ	Dimensionless temperature, $(T-T_C/T_H-T_C)$
ν	Kinematic viscosity, m^2/s

Subscripts

C	Cold
H	Hot
max	maximum
w	wall

showed that vortex shedding is suppressed at height ratio = 0.35 for Re = 13 600 and $\delta/D = 0.8$. Another LDV research by Wu [9] reported $S/D = 0.3$ at Re = 23 000, $\delta/D = 1.5$. Martinetuzzi et al. [10] and Bailey et al. [11,12] reported critical gaps width of $S/D = 0.3$–0.4 at Re = 18 900 and $\delta/D = 0.5$. While Bosch et al. [13] and Taniguchi et al. [14] suggest critical gaps width of $S/D = 0.35$ at Re = 22 000, $\delta/D = 0.13$ and $S/D = 0.5$ at Re = 52 000, $\delta/D = 0.35$ respectively. For a circular cylinder, boundary layer thickness has an important role on gap width unlike square cylinder. Different relation between boundary layer thickness and gap width has reported, Lei et al. [15] reported as boundary layer thickness increase from 0.14 to 0.29, critical gap width decrease from 0.4 to 0.2 whereas Grass et al. [16] suggested a direct relation between boundary layer thickness and critical gap width. They reported as boundary layer thickness (δ/D) increase from 0.28 to 6 critical gap widths varies from 0.25 to 0.5. Taniguchi and Miyakoshi [17] also reported direct relation between boundary layer thickness and critical gap width so that as δ/D vary from 0.34 to 1.05 critical gap width increases from 0.3 to 0.9. However, the mechanism of heat transfer under such asymmetric flow in a channel even for a square cylinder has not been investigated enough. Chakrabarty and Brahma [18] carried out an experimental investigation into the effect of wall proximity on heat transfer and flow field around a rectangular prism for the Reynolds number 4.9×10^4, different blockage ratios, aspect ratios, height-ratios and various angles of attack. They observe that the drag coefficient and local Nusselt number for all blockage ratios and angles of attack decrease as the prism approaches the upper wall. Valencia and Paredes [19] carried out a numerical investigation to analyze flow field and heat transfer in a plane channel with two side by side square bar with different G/d (transverse separation distance between the bars) that was varied from 0 to 5. They reported that for $G/d = 4.5$, 5 the flow is steady because the proximity of the channels walls inhibits the flow instability in those cases. They also shown that secondary peak at time-average local Nusselt number along the channel wall is not seen for steady flow (i.e. $G/d = 5$, 4.5) while for other G/d it can be seen. Rosalesa et al. [20] computed the total drag, lift coefficients and cylinder Nusselt number for unsteady flow field and heat transfer characteristics for a tandem pair of square cylinders in a channel flow. They showed that the drag coefficient and Nusselt number of the cylinder decrease as the heated cylinder approaches the wall.

From the above literature review, effect of wall proximity on flow field and heat transfer was usually studied at high Reynolds number and only for square or circular cylinders. In the present work the numerical investigations are carried out to investigate the effect of wall proximity of a triangular obstacle in the flow field and heat transfer from channel wall in a two-dimensional plane horizontal channel. The goal of this study is to understand the flow structures and fundamental mechanisms of vortex formation in wall proximity near the triangular cylinder on heat transfer from the wall of the channel. Result are presented at Re = 100, 250, 350, 450 and gap width ratios are 0.5, 0.75 and 1. The Prandtl number was consider to be constant at Pr = 0.71.

2. Governing equation

The flow is assumed unsteady, two-dimensional and laminar, for which the governing conservation equations of mass, momentum and energy can be written in the following forms:

$$\frac{\partial u}{\partial x}+\frac{\partial v}{\partial y}=0 \tag{1}$$

$$\frac{\partial u}{\partial \tau}+\frac{u\partial u}{\partial x}+\frac{v\partial u}{\partial y}=-\frac{\partial P}{\partial x}+\frac{1}{\mathrm{Re}}\left(\frac{\partial^2 u}{\partial x^2}+\frac{\partial^2 u}{\partial y^2}\right) \tag{2}$$

$$\frac{\partial v}{\partial \tau}+\frac{u\partial v}{\partial x}+\frac{v\partial v}{\partial y}=-\frac{\partial P}{\partial y}+\frac{1}{\mathrm{Re}}\left(\frac{\partial^2 v}{\partial x^2}+\frac{\partial^2 v}{\partial y^2}\right) \tag{3}$$

$$\frac{\partial \theta}{\partial \tau}+\frac{u\partial \theta}{\partial x}+\frac{v\partial \theta}{\partial y}=\frac{1}{\mathrm{Re}\cdot\mathrm{Pr}}\left(\frac{\partial^2 \theta}{\partial x^2}+\frac{\partial^2 \theta}{\partial y^2}\right) \tag{4}$$

In the above equations u, v, θ, P, Re and Pr are dimensionless fluid velocity, temperature, pressure, Reynolds number and Prandtl number (Pr = 0.71) respectively. The dimensionless forms of the variables are:

$$x=\frac{x^*}{B}, y=\frac{y^*}{B}, \tau=\frac{tu_{\max}}{B}, u=\frac{u^*}{u_{\max}}, v=\frac{v^*}{u_{\max}},$$
$$P=\frac{P^*}{\rho u_{\max}^2}, \theta=\frac{T-T_C}{T_H-T_C} \tag{5}$$

The thermal heat flux exchanged between the walls and the flow is specified by the space-averaged Nusselt number calculated as follows:

$$\overline{\mathrm{Nu}} = \frac{1}{L/B}\int_{o}^{L/B} \mathrm{Nu}\, dx \tag{6}$$

where Nu is the local Nusselt number which is defined as:

$$\mathrm{Nu} = -\frac{\partial\theta}{\partial n} \tag{7}$$

The space- and time-averaged Nusselt number is defined as:

$$\langle\overline{\mathrm{Nu}}\rangle = \frac{1}{t_1}\int_{o}^{t_1} \overline{\mathrm{Nu}}\, dx \tag{8}$$

where t_1 is the total time.

3. Computational domain and boundary condition

The computational domain is shown in Fig. 1. Geometry considered is a horizontal channel with an obstacle isosceles-right triangle placed at the distance "a" from bottom wall. The dimensionless channel length is equal to ($L/B = 30.75$) and the upstream distances, 'Lu', is selected as 8B. The triangle bottom width (B) was selected as H/4 which corresponds to the blockage ratios of 0.25. At the channel inlet, the local normal component of velocity is assumed to be zero, and a fully developed parabolic profile for the axial velocity prescribed:

$$u = u_{\max}\left(1 - \left(\frac{y}{y_B}\right)^2\right),\ v = 0 \tag{9}$$

Where u, v are local components of velocity, and y_B = h. The triangular obstacle, the top wall and the incoming stream are assumed to be in a constant temperature T_C, while the bottom wall is at a temperature T_H so that $T_H > T_C$. No-slip boundary conditions for the velocity are imposed on the upper and lower channel walls and the cylinder surfaces. At outlet the Convective Boundary Condition (CBC) is used that formulated as follow:

$$\frac{\partial\phi}{\partial\tau} + U\frac{\partial\phi}{\partial x} = 0 \tag{10}$$

In above equation, ϕ is any of the dependent variables and U is a mean dimensionless velocity on the outflow.

4. Numerical procedure and validation

The mentioned equations in pervious section are solved by UTFN (Unsteady Turbulent Flow at Non-orthogonal coordinates) code which is a computer code for computation of two-dimensional steady/unsteady and turbulent/laminar flows in FORTRAN. This code has been generated at 2005 by Nourollahi [21]. The finite volume method is applied to transfer the partial differential equations to algebraic relations. Then the SIP (Strongly Implicit Procedure) algorithm is used to solve the obtained algebraic equations. The present code utilize the collocated variable arrangement and use Cartesian velocity components in which all variables are stored at the same control volume. Fig. 2 shows a typical 2D control volume cell for non-orthogonal grid point. Eq. (12) shows the integration form of the generic conservation equation (Eq. (11)) over the finite volume.

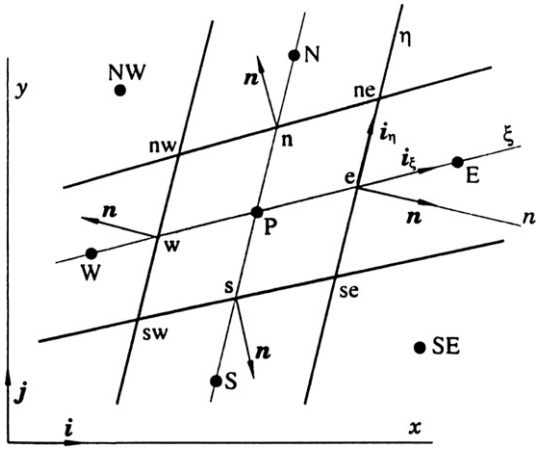

Fig. 2. A typical 2D control volume and the notation used [22].

$$\frac{\partial}{\partial t}(\rho\varphi) + \frac{\partial}{\partial x}(\rho\varphi u) + \frac{\partial}{\partial y}(\rho\varphi v) = \frac{\partial}{\partial x}\left(\Gamma\frac{\partial\varphi}{\partial x}\right) + \frac{\partial}{\partial y}\left(\Gamma\frac{\partial\varphi}{\partial y}\right) + S\varphi \tag{11}$$

$$\frac{\partial}{\partial t}\int \rho\varphi dv + \int_A (\rho\varphi V)\cdot ndA = \int_A (\Gamma grad\varphi)\cdot ndA + \int_V S\cdot dV \tag{12}$$

The principles of finite volume discretization can be found in Ref. [22] and here explains only the discretization of the convection and diffusion terms. At first calculates the mass flux over the faces of the control volume for discretization of the convective term. Only the east side (e) of a control volume (Fig. 2) will be considered; the same approach applies to other faces. The midpoint rule approximation was used to calculate the mass flux.

$$\dot{m}_e = \int_{Ae} (\rho\cdot v\cdot \mathbf{n})dA \approx (\rho\cdot v\cdot \mathbf{n})_e\cdot A_e \tag{13}$$

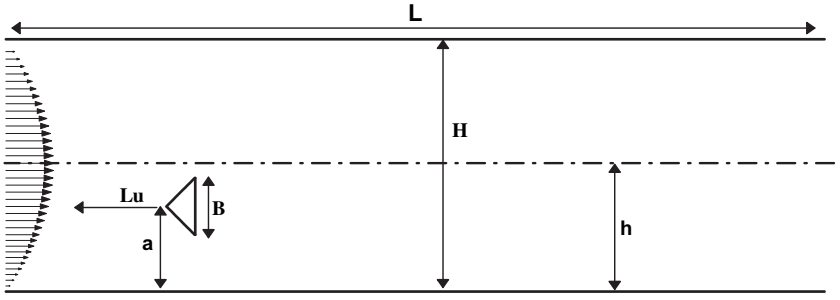

Fig. 1. Geometry of problem.

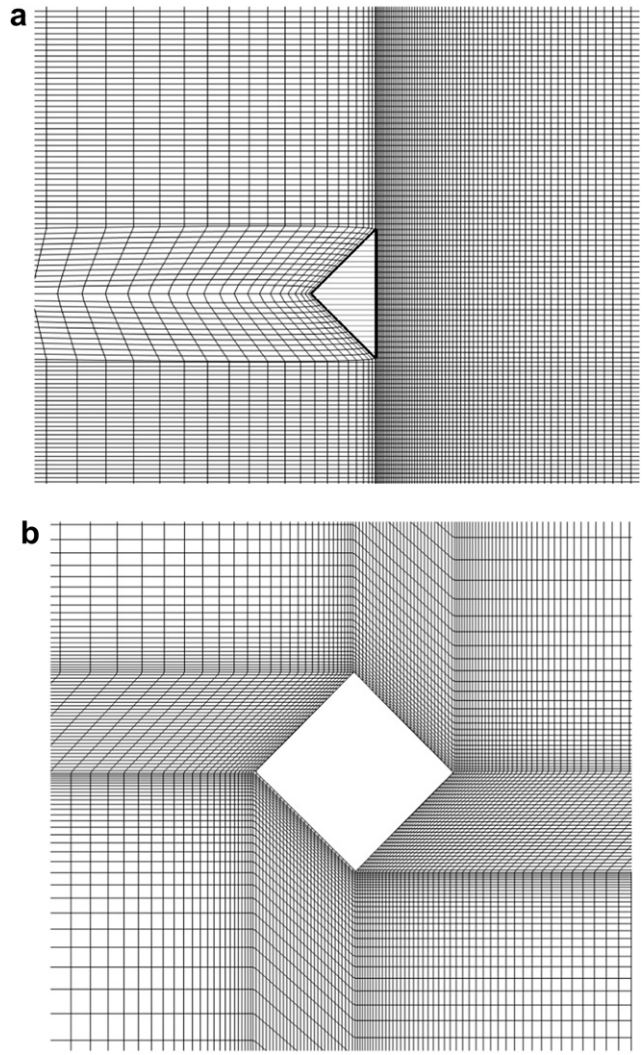

Fig. 3. Non-uniform and non-orthogonal grids over the triangular and inclined square.

A_e is the area of the east face of the control volume. The unit normal vector at the face '*e*' is defined by:

$$n_e A_e = A_e^i i_i \Rightarrow A_e^x i + A_e^y j = (y_{ne} - y_{ns})i - (x_{ne} - x_{ns})j \tag{14}$$

The surface area is:

$$A_e = \sqrt{(A_e^x)^2 + (A_e^y)^2} \tag{15}$$

The expression of the mass flux becomes:

$$\dot{m}_e = \rho_e \left(A^x u + A^Y v\right)_e \tag{16}$$

u and v are the velocity components in x and y directions. The convection flux of any transported quantity is calculated by assuming that the mass flux is known which leads to:

Table 1
Results of grid dependence.

Grid	Δx_{min}, Δy_{min}	$\langle \overline{Nu} \rangle$
145 × 43	0.0312B	3.116
183 × 53	0.02B	3.303
205 × 69	0.012B	3.309

Table 2
Comparison $\langle \overline{Nu} \rangle$ between present work with the previous numerical study [5].

Re	Present study	Abbasi et al. [5]
30	0.71	0.68
100	1.58	1.44
150	2.06	1.96
250	2.62	2.51

$$\int_{Ae} (\rho \cdot \varphi \cdot v) \cdot n dA \approx \dot{m}_e \varphi_e \tag{17}$$

Where $\varphi_e$is the value of φat the center of the cell face. The central difference scheme was used to calculate the φ_e.

The midpoint rule applied to the integrated diffusive flux gives:

$$\int_{A_e} (\Gamma \ grad \ \varphi) \cdot \mathbf{n} dA \approx (\Gamma \ grad \ \varphi \cdot \mathbf{n})_e \cdot A_e \tag{18}$$

The Gauss' theorem was used to calculate derivatives at the cell center and interpolate them to the cell faces. The derivative at the cell center was approximated by the average value over the cell.

$$\left(\frac{\partial \varphi}{\partial x_i}\right)_p \approx \frac{\int_V \left(\frac{\partial \varphi}{\partial x_i}\right) dV}{\partial V} \tag{19}$$

By Gauss' theorem, the volume integral was transformed into a surface integral.

$$\int \frac{\partial \varphi}{\partial x_i} dV = \int_S \varphi i_i \cdot n dS \approx \sum_c \varphi_c S_c^i, \quad c = e, \varphi, w, s \tag{20}$$

For calculating the derivatives at the cell center, the products of φ with the x-components of the surface vectors at all faces of the cell is summed and divided the sum by cell volume;

$$\left(\frac{\partial \varphi}{\partial x_i}\right)_p = \frac{\sum \varphi_c A_c^i}{\delta V}, \ c = e, \varphi, w, s \tag{21}$$

For example to calculate the $\partial\varphi/\partial x$ at the cell center we have:

$$\left(\frac{\partial \varphi}{\partial x}\right)_p = \frac{\varphi_e A_e^x + \varphi_n A_n^x + \varphi_w A_w^x + \varphi_s A_s^x}{\delta V} \tag{22}$$

The φ_e, φ_n, φ_s and φ_w were calculated using the central difference scheme.

In order to solve the Navier-stocks and continuity equations the SIMPLE method providing the pressure-velocity coupling, is used. This method has its origin in staggered grid methodology and is adapted to collocated grid methodology through the use of Rhio & chow interpolation [22]. This interpolation can increase the stability of solution too. The unsteady term is discritized by a three time level

Table 3
Comparison between present work with the previous numerical study [23] of flow over a square cylinder.

Geometry	C_D		Sr	
	Present study	Sohankar et al. [23]	Present study	Sohankar et al. [23]
Square cylinder at $\alpha = 0$ and Re = 100	1.447	1.444	1.40	1.45
Square cylinder at $\alpha = 45$ and Re = 200	1.901	1.944	0.195	0.204

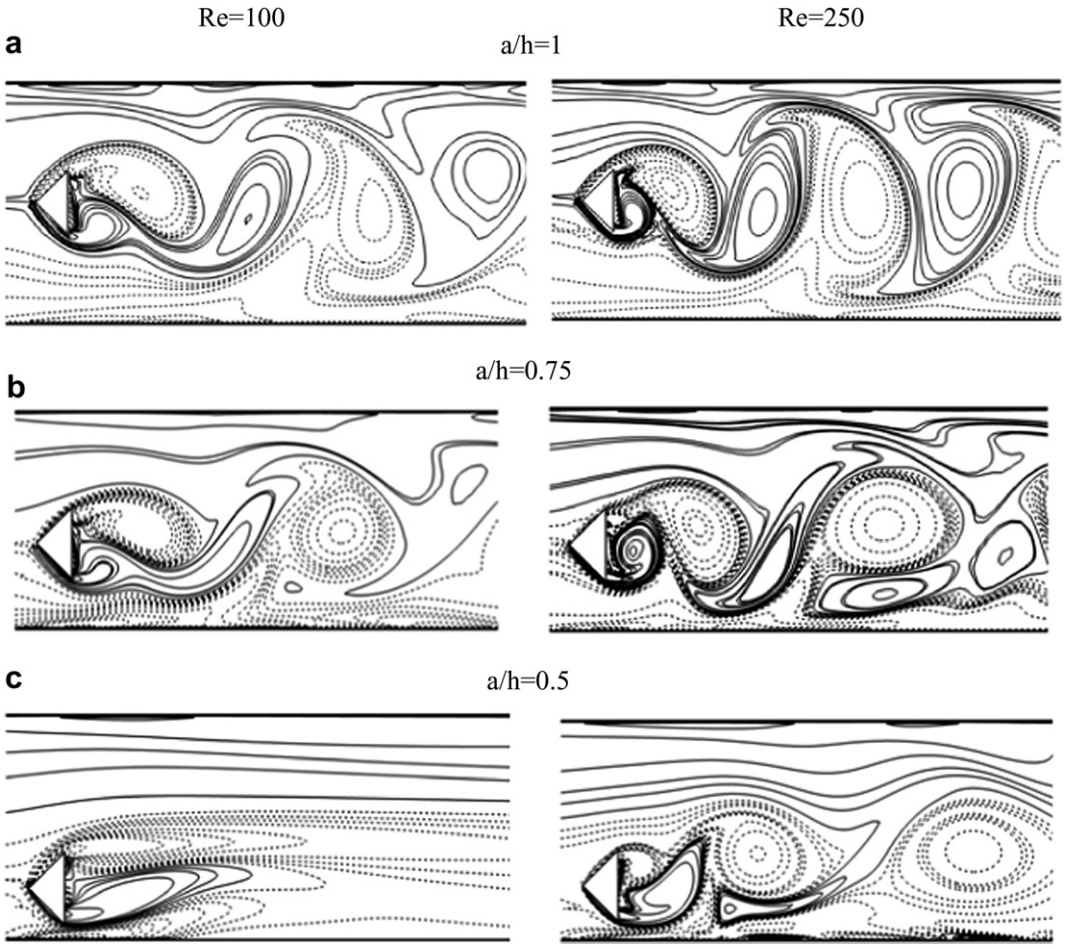

Fig. 4. Instantaneous vorticity contours for Re = 100 (left), and Re = 250 (right) at different gap width ratios.

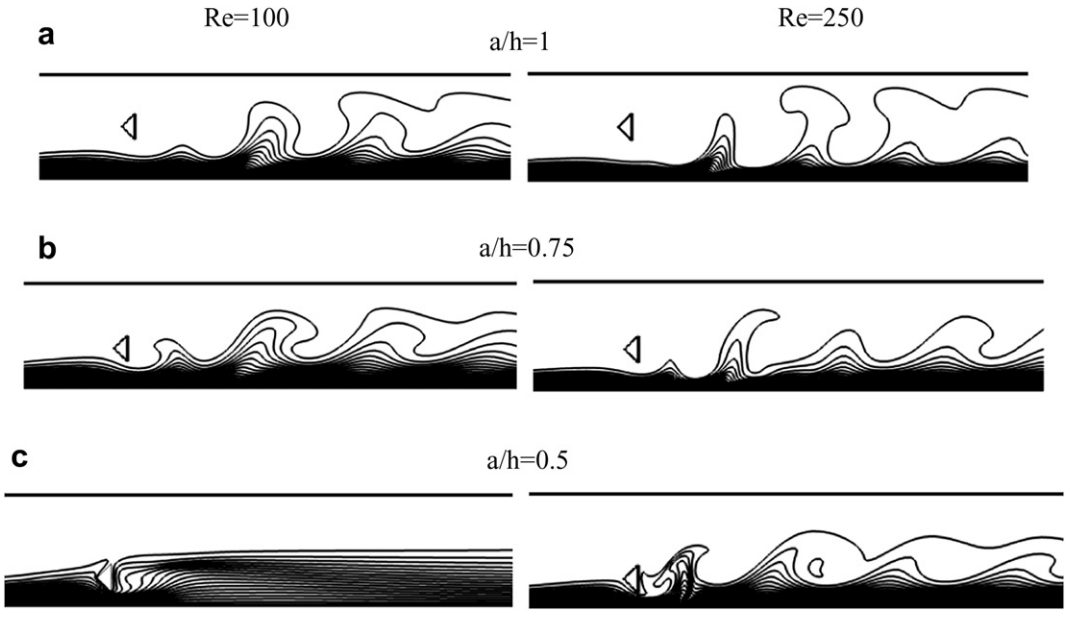

Fig. 5. Instantaneous temperature contours for Re = 100 (left), and Re = 250 (right) at different gap width ratios.

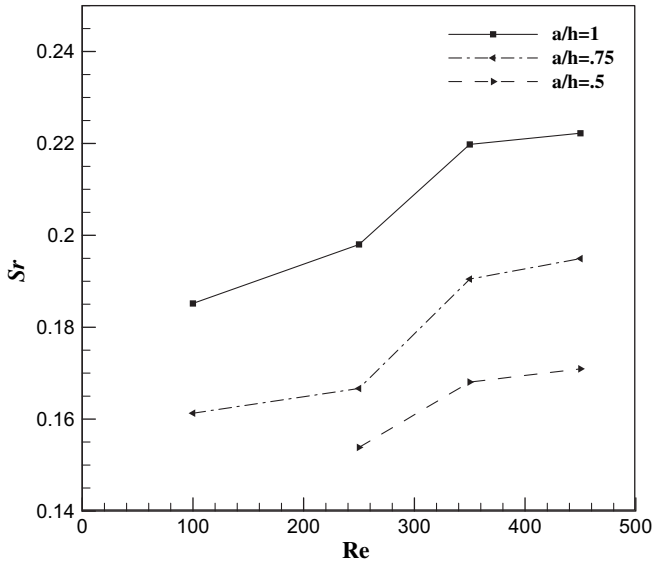

Fig. 6. Variation of Strouhal number with Reynolds number at different width ratios.

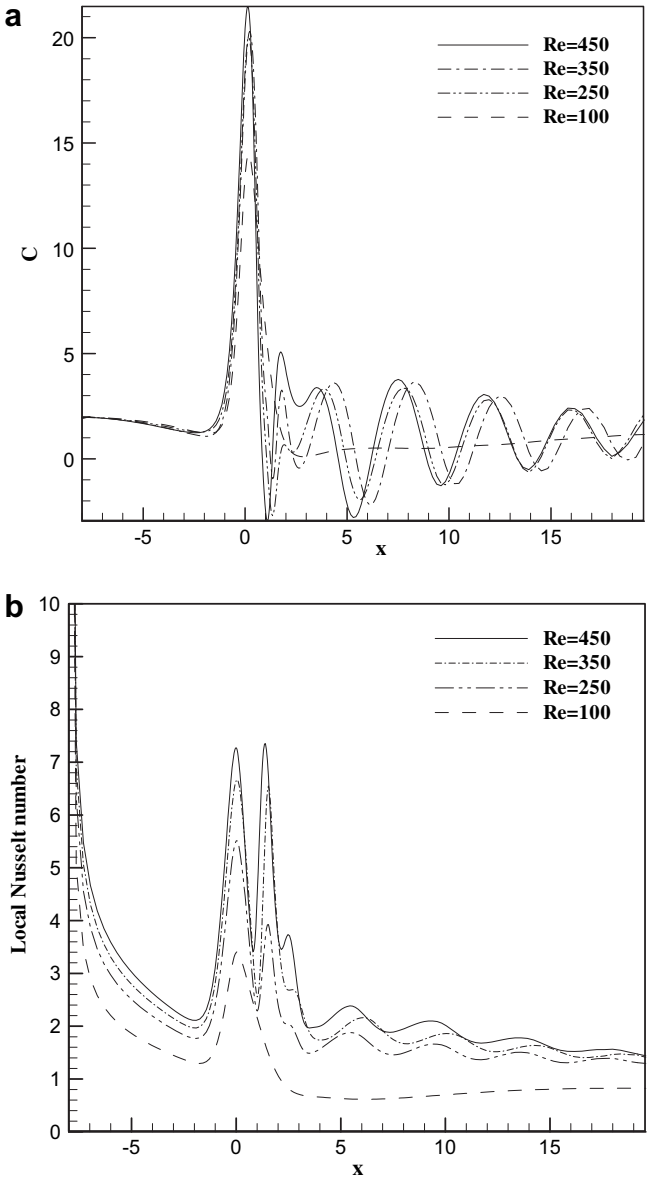

Fig. 7. Distribution of instantaneous (a) local skin friction coefficient and (b) local Nusselt number along the bottom wall of channel for a/h = 0.5 at different Reynolds number.

method. In addition three different discretization schemes are available to approximate the convective terms, Upwind/Central Difference and Hybrid schemes. Diffusion term is discritized by CDS. In this study, The Convection and Diffusion terms of the equations are discretized by Central Difference Scheme (CDS). Further details about the numerical method are given in Nourollahi [21].

A non-uniform grid that is non-orthogonal before the obstacle is used with a minimum spacing near the walls and stretching with the fix factor (Fig. 3a). To check grid independence in this work the case with one triangular obstacle in the middle of channel at Re = 450 is solved. Table 1 shows the results of grid dependency for time and space-averaged Nusselt number. Results show that, when the number of grid points pass from a 145 × 43 to 183 × 53 and then to 205 × 69, the space- and time-average Nusselt number increases 6% and 0.2% respectively. These grid points have minimum grid spacing 0.0312B, 0.02B and 0.012B for 145 × 43, 183 × 53 and 205 × 69 respectively. Therefore the minimum grid spacing 0.02B is sufficient and is retained for other investigations.

This case corresponds to the work of Abbassi et al. [5]. The nature of the flow field shows a similarity behavior. Table 2 shows the time and space-averaged Nusselt number over the lower wall of the channel. It can be observed a reasonable agreement between the results of this program and the previous studies. For better validation of the UTFN code, the flow over a square cylinder at incidence ($\alpha = 0$ and 45(Fig. 3b)) was studied in the free stream flow. The results of the present work compared with the previous published work (Sohankare et al. [23]) which is shown in Table 3. The results show a good agreement in comparison with Ref. [23].

5. Results and discussion

The effect of wall proximity of a triangular obstacle on the flow field and the heat transfer in a horizontal channel was investigated numerically. The obstacle with the sharp edges has a special effect on vortex formation in flow field. It can be say that the position of obstacle in wall proximity is also effective over the formation of vortex. Fig. 4 shows instantaneous vorticity contours for three difference gap width ratios at Re = 100 and Re = 250. With decreasing the gap width ratio, vortex shedding decreases and then fades away at lower Reynolds number. This phenomenon can be observed in Fig. 4c for a/h = 0.5 at Re = 100. With increasing the momentum force at higher Reynolds number, the wall damping effect on the vortex generation disappears (Fig. 4c at Re = 250). With increasing the distance between obstacle and channel's wall, vortex shedding is created at the downstream of the obstacle.

Instantaneous temperature contours are shown in Fig. 5. In this figure, the effect of gap width ratio and Reynolds number on temperature distribution can be observed. As expected, the flow field has a main effect on convective heat transfer. It is observed that for both Re = 100 and Re = 250 vortex shedding causes the diffusion of energy to increase in the flow field whereas for a/h = 0.5 at Re = 100. There is only a contraction of isothermal lines at the place of obstacle, but presence of the obstacle does not has any effect on heat transfer to medium flow in comparison with the periodic flow (i.e. a/h = 1, 0.75) (see the Fig. 5c at Re = 100). While obstacle has just a little local effect on heat transfer from the channel wall at Re = 100 for a/h = 0.5 just like Re < 45 for a/h = 1 [5].

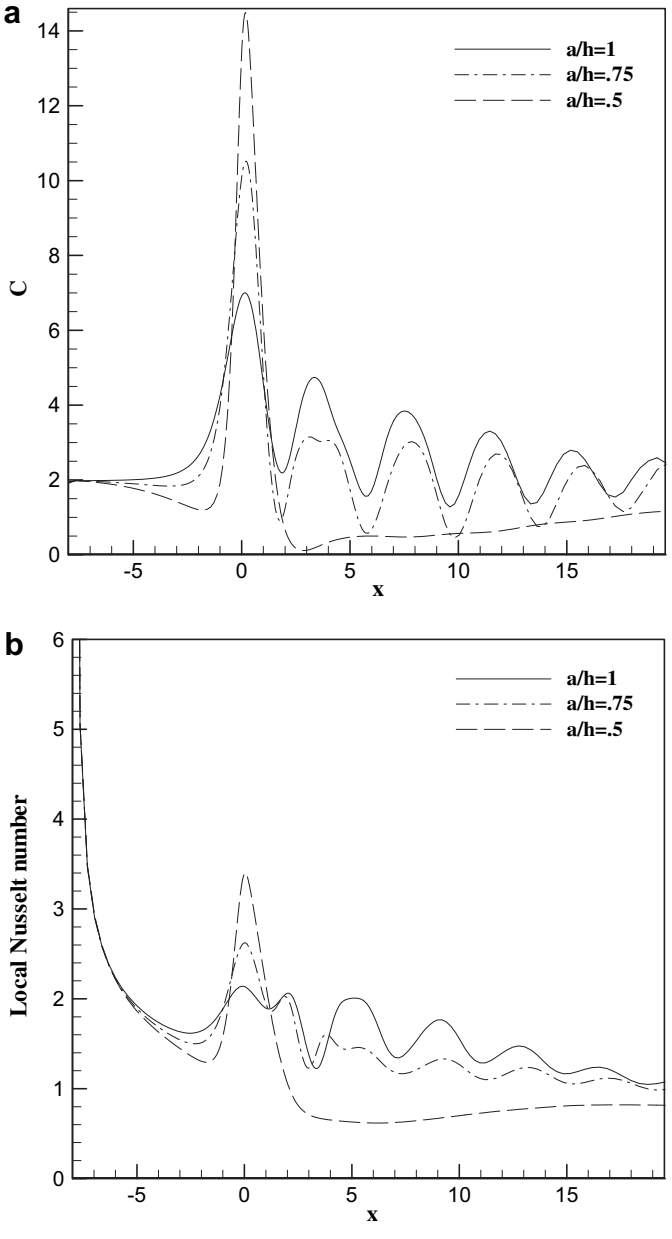

Fig. 8. Distribution of instantaneous (a) local skin friction and (b) local Nusselt number along the bottom wall of channel for three gap width ratios at Re = 100.

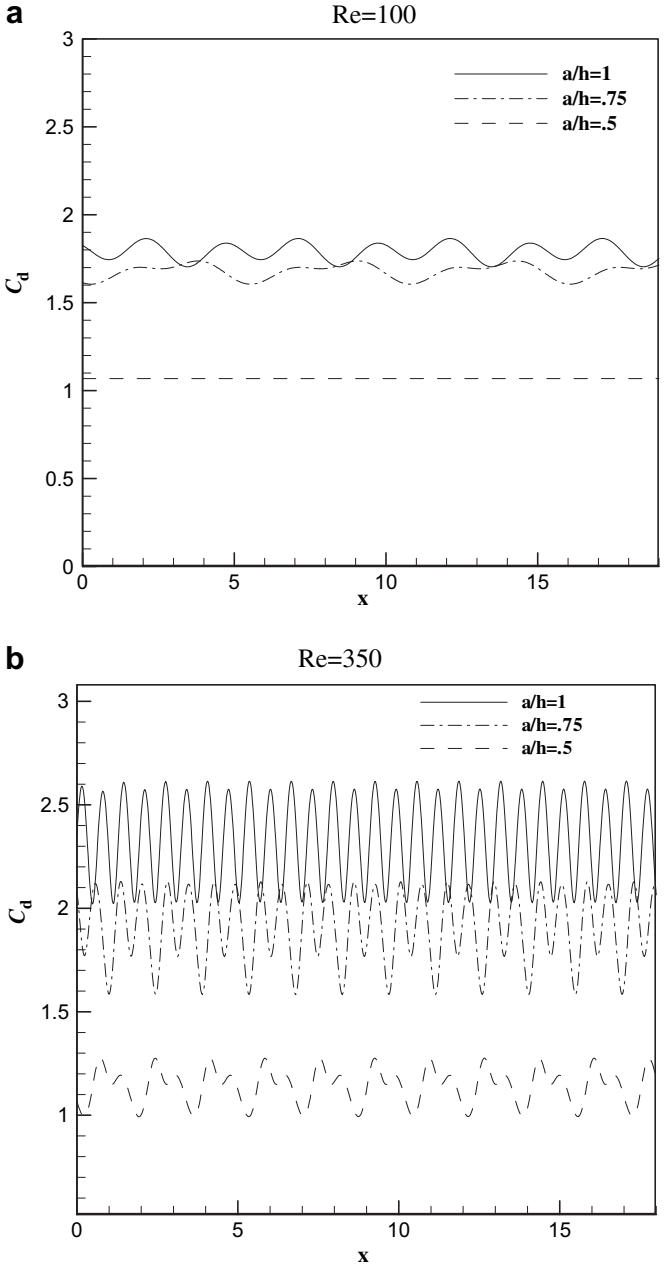

Fig. 9. Instantaneous drag coefficient for three gap width ratios at different Reynolds number.

On the main parameter in the unsteady flow field is the frequency of the vortex shedding. Fig. 6 shows the variation of Sr number with Reynolds number at different wall proximity. It is observed that the approaching to the wall, Sr number decreases and become zero for wall proximity equal 0.5 at Re = 100. The presented results show a good agreement in comparison with the results of Abbassi et al. [5] for a/h = 1. Variation of the vortex formation has a strong effect on the skin friction coefficient and heat transfer rate. Fig. 7 shows distribution of instantaneous modified local skin friction coefficient ($C = C_f \cdot \mathrm{Re}$) and local Nusselt number along the lower plate for gap width ratio a/h = 0.5 at different Reynolds numbers. It can be observed that there is not sensitive changed on the modified local skin friction coefficient and local Nusselt number at the upstream of the obstacle. It is due to the flow field at the upstream of the obstacle which is not affected so the variation of the C and Nu number are limited. The vortex regions at the downstream of the triangular cylinder create a large variation over the Nusselt number. The obstacle separates the flow over the lower channel wall, so heat transfer rate increases. With going toward the end of the channel, the vortexes in the flow field disappear so the mixing decreases and subsequently Nusselt number reduces. This phenomenon caused the periodic variation of the modified local skin friction coefficient on the wall of the channel. It should be mentioned that the increasing the Reynolds number does not have a great effect on the local Nusselt number and modified local skin friction coefficient except Re = 100 (See Fig. 8). When the obstacle is placed in the center of channel, periodic motion will cause periodic nature in local Nusselt number. As obstacle approaches the wall asymmetric condition will be governed and inhibit fluctuation in local Nusselt number. It is evident that at the place of obstacle there is a large increase in both C and Nu

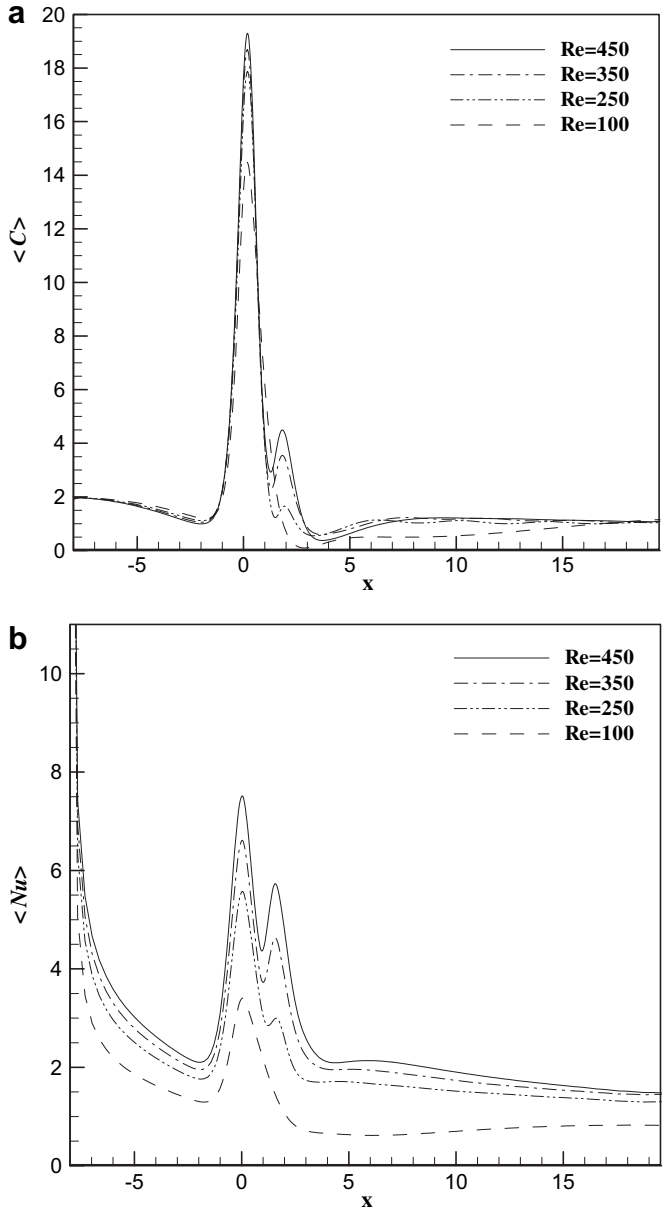

Fig. 10. Distribution of time-averaged (a) skin friction coefficient and (b) local Nusselt number along the bottom wall of channel for a/h = 0.5 at different Reynolds number.

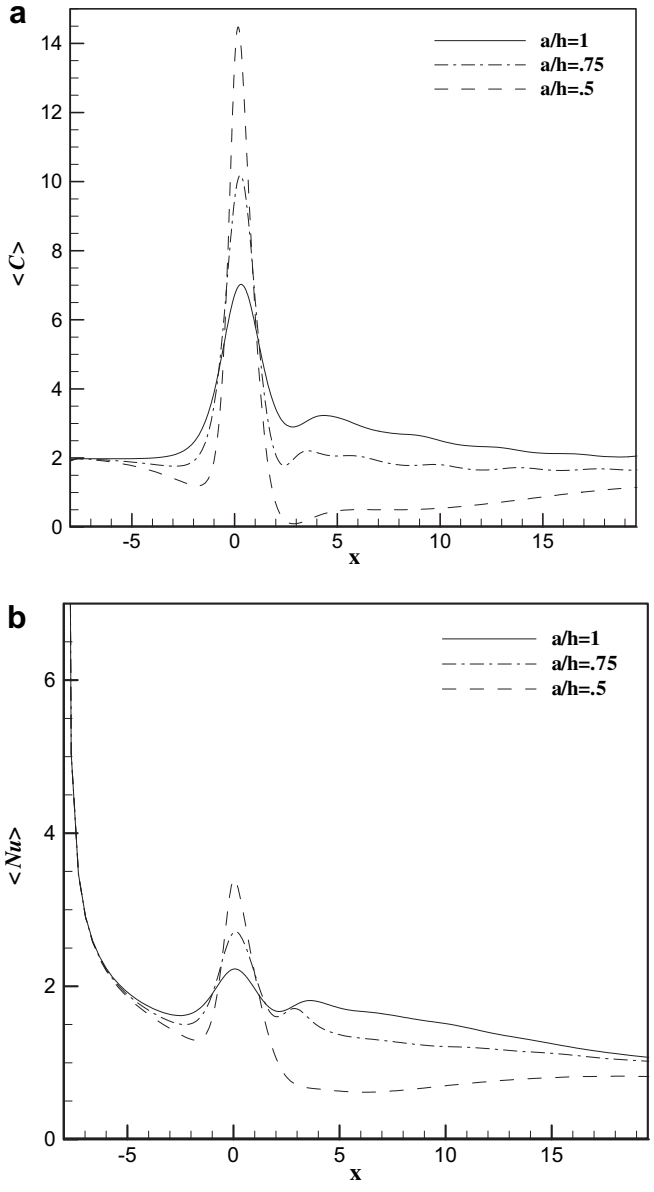

Fig. 11. Distribution of time-averaged (a) local skin friction coefficient and (b) local Nusselt number with along the bottom wall of channel for three gap width ratios at Re = 100.

number that is maximum for a/h = 0.5 and minimum for a/h = 1.0 but at the downstream is to be inversed.

One of the main wall proximity effects on the obstacles is over the drag coefficient. With formation of vortex, pressure distribution at the downstream of the obstacle is changed and this variation has a strong effect over the pressure drag. Instantaneous drag coefficients for three different height ratio at Re = 100 and Re = 350 are shown at Fig. 9. With approaching the obstacle to the wall, vortex shedding remove so drag coefficient decreases at low Reynolds number. On the other hand, for a/h = 0.75 and 1.0 vortex shedding creates the high pressure drag over the triangular obstacle. With increasing the Reynolds number, although the vortex shedding appears at a/h = 0.5 but it does not have a sensitive effect over the pressure distribution at the downstream of the obstacle. So it has only effect on the amplitude of the drag coefficient.

Time-average of modified local skin friction coefficient $\langle C\rangle = \langle C_f \cdot \mathrm{Re}\rangle$ and local Nusselt number along bottom wall of the channel are presented in Figs. 10 and 11 for different gap width ratios and Reynolds numbers. There is a sudden change in both <c> and <Nu> at the downstream of the obstacle. The formation of the small recirculation region over the wall of the channel after the obstacle causes the secondary peak except for Re = 100. This secondary peak has also been reported for high Reynolds number by Chattopadhyay [6]. Streamwise and time-averaged modified skin friction and Nusselt number are show in Fig. 12. It is observed that when the obstacle goes away the wall of the channel, Nusselt number increases. This increasing for the Nusselt number is due to the vortex creation at surface of the channel wall. Heat transfer rate increases with increasing the Reynolds number. The heat transfer enhancement approximately 100 percentage until Re = 350. For Reynolds number bigger than 350, the rate of heat transfer enhancement decreases. It is due to the limitation of the mixing effect on the Nusselt number.

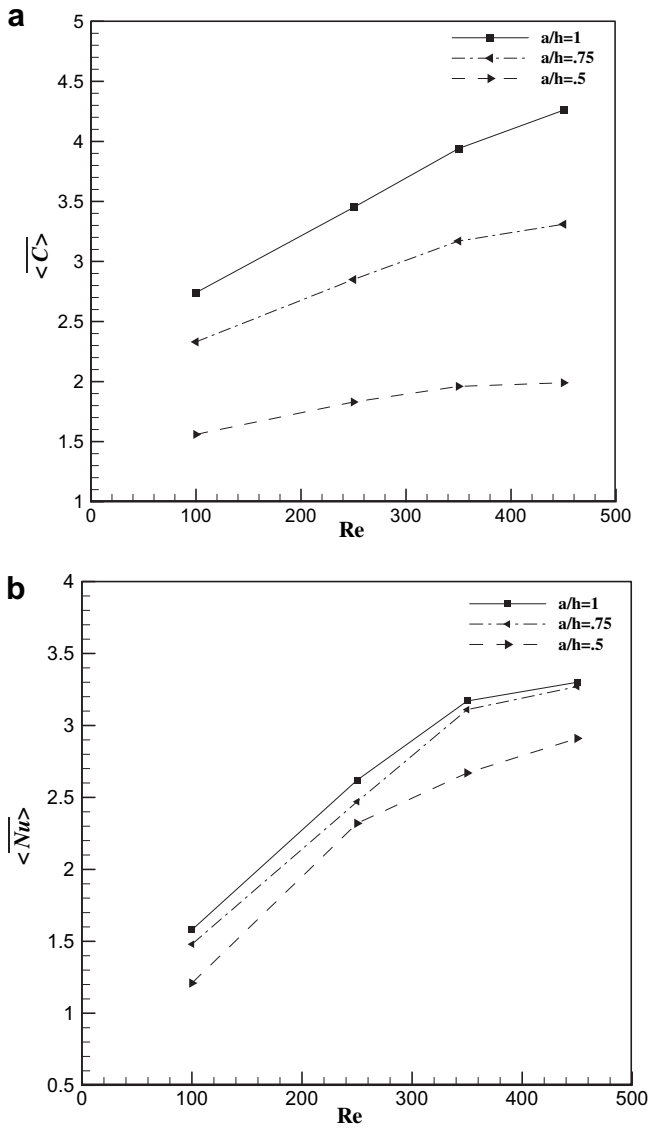

Fig. 12. Distribution of streamwise and time-averaged (a) skin friction coefficient and (b) Nusselt number with Reynolds number for different gap width ratios.

It should be mentioned that Variation of the modified skin friction coefficient in comparison with the Nusselt number is observable and wall proximity has a significant effect over the C more than Nu number. The Reynolds number has not significant effect on the modified skin friction at a/h = 0.5. With increasing the gap width ratio, Reynolds number has an observable effect over the pressure distribution at the downstream of the triangular cylinder, so the C increases remarkable.

6. Conclusion

The effect of wall proximity of a triangular obstacle on fluid flow and heat transfer was investigated numerically in a horizontal plane channel. Results show that the vortex formation at the downstream of the obstacle has a main effect on the flow separation over the surface of the lower channel wall. By approaching triangular cylinder in the wall, removes vortex shedding and subsequently the heat transfer rate decreases at low Reynolds number. Results show that the variation of vortex formation has a more significant suppression effect on the skin friction coefficient than the Nusselt number. As the obstacle approaches the wall drag coefficient has an observable reducing.

References

[1] A.E. Bergles, Techniques to augment heat transfer, in: Handbook of Heat Transfer Applications. McGraw-Hill, New York, 1983, pp. 31–80.
[2] G. Biswas, H. Chattopadhyay, Heat transfer in a channel with built-in wing type vortex generators. Int. J. Heat Mass Transfer 35 (1992) 803–814.
[3] G. Wang, K. Stone, S.P. Vanka, Unsteady heat transfer in baffled channel. Heat and Mass Transfer 118 (1996) 585–591.
[4] A. Valencia, Numerical study of self-sustained oscillatory flows and heat transfer in channels with a tandem of transverse vortex generators. Heat and Mass Transfer 33 (1998) 465–470.
[5] H. Abbassi, S.B. Turki, S. Nasrallah, Numerical investigation of forced convection in a plane channel with a built-in triangular prism. Int. J. Thermal Sci. 40 (2001) 649–658.
[6] H. Chattopadhyay, Augmentation of heat transfer in a channel using a triangular prism. Int. J. Thermal Sci. 46 (2007) 501–505.
[7] E. Ulrichs, H. Herwig, Between two limits: flow separation behind a bluff body close to a wall. Forschung im Ingenieurwesen 68 (2003) 36–38 Springer-Verlag.
[8] D.F.G. Durao, P.S.T. Gouveia, J.C.F. Pereira, Velocity characteristics of the flow around a square cross-section cylinder placed near a channel wall. Exp. Fluids 11 (1991) 298–304.
[9] K.C.Q. Wu, An experimental investigation of the flow around a two-dimensional cylinder in the proximity of a solid wall: effect of the gap size. MESc thesis, Faculty of Engineering Science, The University of WesternOntario, London, Canada, 1999.
[10] R.J. Martinuzzi, S.C.C. Bailey, G.A. Kopp, Influence of wall proximity on vortex shedding from a square cylinder. Exp. Fluids 34 (2003) 585–596.
[11] S.C.C. Bailey, G.A. Kopp, R.J. Martinuzzi, Vortex shedding regime from a square cylinder near a wall. J. Turbulence 3 (3) (2002) 1–18.
[12] S.C.C. Bailey, R.J. Martinuzzi, G.A. Kopp, The effects of wall proximity on vortex shedding from a square cylinder: three dimensional, effects. Phys. Fluids 14 (2002) 4160–4177.
[13] G. Bosch, M. Kappler, V. Rodi, Experiments on the flow past a square cylinder placed near a wall. Exp. Thermal Fluid Sci. 13 (1996) 292–305.
[14] S. Tamaguchi, K. Miyakoshi, S. Dohda, Interference between plane wall and two-dimensional rectangular cylinder (fluid force when the angle of attack is 0 deg). Trans. JSME 49 (1983) 2522–2529.
[15] C. Lei, L. Cheng, K. Kavanagh, Re-examination of the effect of a plane boundary on force and vortex shedding of a circular cylinder. J. Wind Eng. Ind. Aero 80 (1999) 263–286.
[16] A.J. Grass, P.W.J. Raven, R.J. Stuart, J.A. Bray, The influence of boundary layer velocity gradients and bed proximity on vortex shedding from free spanning pipelines. Trans. ASME 106 (1984) 70–78.
[17] S. Taniguchi, K. Miyakoshi, Fluctuating fluid forces acting on a circular cylinder and interference with a plane wall. Exp. Fluids 9 (1990) 197–204.
[18] D. Chakrabarty, R.K. Brahma, Effect of wall proximity in fluid flow and heat transfer from a rectangular prism placed inside a wind tunnel. Int. J. Heat Mass Transfer 51 (2008) 736–746.
[19] A. Valencia, R. Paredes, Laminar flow and heat transfer in confined channel flow past square bars arranged side by side. Heat and Mass Transfer 39 (2003) 721–728.
[20] J.L. Rosales, A. Ortega, J.A.C. Humphrey, A numerical simulation of the convective heat transfer in confined channel flow past square cylinders: comparison of inline and offset tandem pairs. Int. J. Heat Mass Transfer 44 (2001) 587–603.
[21] M. Nourollahi, Generation of CFD code for solving the fluid governing equations in non-orthogonal coordinate systems. MSc. thesis, Faculty of Mechanical Engineering, Babol Noshirvani University of Technology, Babol, Iran, 2007.
[22] Joel H. Ferziger, M. Peric, Computational Methods for Fluid Dynamics. Springer-Verlag, Berlin Heidelberg, New York, 2002.
[23] A. Sohankar, C. Norberg, L. Davidson, Low-reynolds number flow around a square cylinder at incidence: study of blockage, onset of vortex shedding and outlet boundary condition. Int. J. Num. Methods Fluids 26 (1998) 39–56.